Radio-frequency spectroscopy of the attractive Hubbard model in a trap

Sanjoy Datta,[1,2,*] Viveka Nand Singh,[1] and Pinaki Majumdar[1,†]
[1]*Harish-Chandra Research Institute, Chhatnag Road, Jhusi, Allahabad 211019, India*
[2]*Institut Néel and Laboratoire de Physique et Modélisation des Milieux Condensés, Université Grenoble I and CNRS, B.P. 166, 38042 Grenoble, France*
(Received 21 August 2013; revised manuscript received 29 April 2014; published 9 May 2014)

Attractive interaction between fermions can lead to pairing and superfluidity in an optical lattice. In contrast to the "continuum," on a lattice the trap-induced density variation can generate a non monotonic profile of the pairing amplitude and completely modify the spectral signatures of any possible pseudogap phase. Using a tool that fully captures the inhomogeneity and strong thermal fluctuations, we demonstrate how the crucial radio-frequency signatures of pairing in a trapped attractive fermion lattice are "inverted" compared to the traditional continuum case. These features would be central in interpreting any spectroscopic hint of fermion pairing and superfluidity.

DOI: 10.1103/PhysRevA.89.053609 PACS number(s): 67.85.−d, 37.10.Jk, 71.27.+a, 75.10.Lp

I. INTRODUCTION

Optical lattices allow controllable cold atom realization [1–4] of interacting quantum lattice models. The achievements include the observation of a Fermi surface [5] and Mott insulating phase [6,7] for repulsive fermions, and the evidence of superfluidity (SF) [8] and anomalous expansion [9] in the attractive case. While the canonical antiferromagnetic state [10,11] of repulsive fermions and superfluidity in the single-band attractive Hubbard model (AHM) [12] remain inaccessible, the observation of *precursors* [13] to these states would already be a major advance.

Even if a pairing-induced gapped, or pseudogap (PG), phase is thermally accessible, the spectroscopic signatures would be hard to interpret. The well-developed theory of pairing in the "flat" AHM [14–16] provides no obvious guidance on the angle-resolved spectrum of the trapped lattice. The complication has a simple origin. Trapping potentials lead to a monotonic increase in density, as one moves from the edge to the center of the trap, but the *pairing amplitude* variation becomes nonmonotonic once the central density crosses unity. The nonmonotonicity affects the spatial character of excitations and generates a spectroscopic response differing drastically from the famed "backbending" that one observes in the flat lattice or the trapped continuum gas [17,18].

We completely solve this problem, using a Monte Carlo (MC) method that handles both the inhomogeneity and thermal fluctuation on large lattices. We predict the following: (1) Increasing confinement leads to rapid decrease in the overall spectral gap, pushing weight to low frequency, and quick suppression of the coherence feature at the gap edge. (2) Radio frequency spectroscopy (RFS), the cold atom analog of angle resolved photoemission spectroscopy (ARPES), shows "backbending," the traditional signature of a pairing gap, only for weak trapping and low temperature, with the momentum-dependent gap smallest near $\mathbf{k} \sim \mathbf{k}_F \sim \{\pi/2,\pi/2\}$. For stronger confinement, however, this inverts to "forward bending" with the gap largest near $\mathbf{k} \sim \mathbf{k}_F$, *despite the presence of strong pairing*. (3) This "inversion" is *generic* and arises when the density at the trap center exceeds 1. It survives beyond T_c but vanishes for $T \gg T_c$.

We provide an analysis of the effect in terms of the quasiparticle states in the trap and demonstrate an approximate "local density" approach that captures most of the MC-based features and can yield reliable RF spectra on very large, experimentally relevant, lattices.

II. MODEL HAMILTONIAN AND METHOD

We study the two-dimensional (2D) attractive Hubbard model in the presence of a harmonic potential:

$$H = H_0 - |U| \sum_i n_{i\uparrow} n_{i\downarrow}, \tag{1}$$

where

$$H_0 = -t \sum_{\langle ij\rangle\sigma} c^\dagger_{i\sigma} c_{j\sigma} + \sum_{i\sigma} (V_i - \mu) n_{i\sigma}. \tag{2}$$

The first term denotes the nearest neighbor tunneling amplitude of atoms on the optical lattice, the confining potential has form $V_i = V_0(x_i^2 + y_i^2)$, μ is the chemical potential, and $U > 0$ is the strength of attractive on-site interaction. x_i and y_i are measured in units of lattice spacing a. On a $L \times L$ lattice, the corner value $V_c = V_{\{L/2,L/2\}} = 2V_0(La/2)^2$. We use $L = 24$.

The spatial variation in mean value and the thermal fluctuation about the mean pairing amplitude are crucial in describing the physics of this system. Unbiased calculations in the homogeneous limit employ determinantal quantum Monte Carlo (DQMC) [14–16] to access finite temperature properties. While there are a few recent calculations using large system size [11,20,21], they are focused on thermodynamic properties and have not touched upon the spectral functions of the AHM.

We use a strategy used earlier on moderately sized systems [22,23], augmented by a cluster Monte Carlo technique [24] that readily allows access to system size $\sim 30 \times 30$. We first derive an effective Hamiltonian by decoupling the interaction term simultaneously [25] in the pairing and density channels via a Hubbard-Stratonovich (HS) transformation. The exact transformation puts a constraint on the coupling constants in these two channels [26]. We choose both couplings to be unity and neglect the time dependence of the auxiliary fields, to reproduce Hartree-Fock-Bogoliubov-de Gennes (HFBdG)

*sanjoy.datta@grenoble.cnrs.fr
†pinaki@hri.res.in

theory at $T = 0$. Our model is

$$H_{\rm eff} = H_0 + H_{\rm coup} + H_{\rm stiff}, \tag{3}$$

where

$$H_{\rm coup} = \sum_i (\Delta_i c^\dagger_{i\uparrow} c^\dagger_{i\downarrow} + \Delta^\star_i c_{i\downarrow} c_{i\uparrow}) - \sum_i \phi_i n_i \tag{4}$$

and

$$H_{\rm stiff} = \frac{1}{U} \sum_i \left(|\Delta_i|^2 + \phi_i^2\right). \tag{5}$$

$\Delta_i = |\Delta_i| e^{i\theta_i}$ is a complex scalar, and ϕ_i is a real scalar field. The inclusion of ϕ_i is essential to capture the Hartree shift in the inhomogeneous system. The $T = 0$ state corresponds to solving $\delta\mathcal{E}/\delta\Delta_i = 0$ and $\delta\mathcal{E}/\delta\phi_i = 0$, where $\mathcal{E}$ is the energy in the $\{\Delta,\phi\}$ background and reproduces mean field theory [27]. Finite temperature configurations $\{\Delta_i,\phi_i\}$ follow the distribution $P\{\Delta_i,\phi_i\} \propto {\rm Tr}_{c,c^\dagger} e^{-\beta H_{\rm eff}}$ and may differ significantly from the mean field state.

We use the Metropolis algorithm to update the $|\Delta|$, θ, and ϕ variables. This involves solution of the HFBdG equation [27,28] for each attempted update, to compute the fermion trace. For determining the acceptance of a move we solve the HFBdG equation on a 8×8 cluster around the update site. Global properties like pairing field correlation, density of states, etc., are computed via solution of the HFBdG equation on the full 24×24 system in equilibrium $\{\Delta_i,\phi_i\}$ configurations. We have checked (see Sec. V A) that our T_c matches the DQMC estimate [16] over a wide U/t window. Large-scale determinantal Monte Carlo (DQMC) results are not available for the trapped problem, so we compared the results of our method to DQMC data in the "flat" problem. DQMC results for the superfluid transition temperature (T_c) are available at density $n = 0.7$ on a 10×10 lattice for U/t varying from 2 to 8.

III. SPATIAL BEHAVIOR AT FINITE TEMPERATURE

The parameter space of the trap problem involves U/t, V_c/t, average density $n_{\rm av}$, and temperature T/t. To keep the effort manageable we set $U/t = 6$, where the T_c in the flat system is maximum. We have explored the variation from weak to strong confinement over a wide density window but will show detailed results mainly at $n_{\rm av} = 1$.

For $V_0 = 0$ the model is known [14,15] to have a SF ground state for $0 < n < 2$, except at $n = 1$ where there is coexistence of SF and DW correlations. For $n \neq 1$ the SF has Bardeen-Cooper-Schrieffer (BCS) character at $U/t \ll 1$ and a Bose-Einstein condensed (BEC) form at $U/t \gg 1$. What is the effect of confinement?

Figure 1(a) shows the ground state for varying $n_{\rm av} = N_f/L^2$, where N_f is the number of fermions, and corner potential V_c. At finite V there is a small window near $n_{\rm av} = 1$ where DW correlations survive, up to $V_c/t \sim 0.8$ [29]. Beyond this window the system has only SF order. However, the spatial extent of the SF shrinks with increasing V_c or $n_{\rm av}$ since the central part of the trap becomes doubly occupied ($n_i = 2$) suppressing Δ_i. Figure 1(b) shows the V_c-T phase diagram at $n_{\rm av} = 1$. There is a narrow SF+DW window at small V_c, beyond which there is only SF order, with the T_c (left axis)

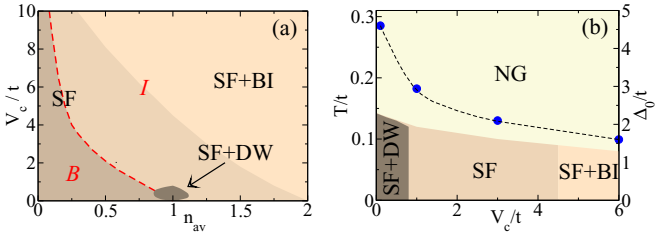

FIG. 1. (Color online) (a) Ground state of the 2D AHM at $U/t = 6$ for varying average dimensionless density $n_{\rm av}$ and trapping strength V_c/t. The tiny region near $n_{\rm av} = 1$ corresponds to strong density wave (DW) correlation coexisting with superfluidity [19]. The band insulator (BI) refers to the presence of a $n_i = 2$ core. The B and I regions, separated by the red dotted line, correspond to "backbended" and "inverted" RFS. (b) Finite temperature phase diagram at $U/t = 6$ and $n_{\rm av} = 1$. Beyond the small window at weak V_c the system has only SF order at low temperature, with an increasing BI core for $V_c/t \gtrsim 4$. NG refers to the gapped normal state. The T_c (on left axis) falls monotonically with V_c as does Δ_0/t (blue dots, right axis); the $T = 0$ gap in the spectrum. The dotted line is a guide to the eye. The T_c at $V_c = 0$ would vanish in the infinite volume limit; the results here are for a 24×24 system.

decreasing quickly with increasing confinement. The $T = 0$ spectral gap Δ_0 (right axis) falls even more sharply, dropping from $\sim 4.6t$ at $V_c = 0$ to $\sim 1.5t$ at $V_c = 6t$.

Figure 2 shows the radial variation of the thermal average of $n_i = \sum_\sigma c^\dagger_{i\sigma} c_{i\sigma}$ (left), $|\Delta_i|$ (center), and $\Phi_i = |\Delta_i||\Delta_{i+\delta}| \cos(\theta_i - \theta_{i+\delta})$ (right). The coordinate i is $r = \sqrt{x^2 + y^2}/(L/\sqrt{2})$, varying along the diagonal. Φ_i tracks nearest neighbor correlation in that direction. We have set $V_c = 3t$ and $n_{\rm av} \sim 1$ and $T = 0, 0.08t, 0.3t$.

Figure 2(a) shows the expected monotonic fall in $\langle\langle n_r \rangle\rangle$ at all T. The cloud at $T = 0.3t$ is slightly broader than at $T = 0$. The pairing field amplitude in Fig. 2(b) is more interesting. It is nonmonotonic at all T, a peculiarity of the lattice where it grows with n till $n = 1$ and falls beyond. The $T = 0$ result for $\langle|\Delta_r|\rangle$ is what is expected from mean field HFBdG theory, with a clear peak in the region where $n_r \sim 1$. At $T = 0.08t$ the amplitude profile looks similar to $T = 0$, but with a large growth in the corner where it was zero at $T = 0$! The trend amplifies at $T = 0.3t$ where $\langle\langle|\Delta_r|\rangle\rangle$ is much less inhomogeneous than at $T = 0$. This is due to the low-amplitude stiffness in regions with low $|\Delta_i|$ at $T = 0$. We provide a connection to the flat system physics in Sec. V B.

Figure 2(c) is meant to highlight the suppression of phase correlation with temperature. At $T = 0$ the phases are locked, so $\Phi_i = |\Delta_i||\Delta_{i+\delta}| \approx |\Delta_i|^2$. At $T = 0.08t \sim 0.7T_c$ while the amplitudes are not very different from $T = 0$ the phase correlation is weakened. By $T = 0.3t$ while amplitudes have grown, NN phase correlations have weakened to about 20% of the $T = 0$ value. Long-range phase correlation is of course lost at T_c. These spatial characteristics are not directly measurable, experimentally, so we move to the spectral signatures that RF spectroscopy can probe.

Figure 3 shows the single particle density of states (DOS). Figure 3(a) shows V_c dependence at $T = 0$. There are two primary effects of trapping: (1) the effective gap reduces with

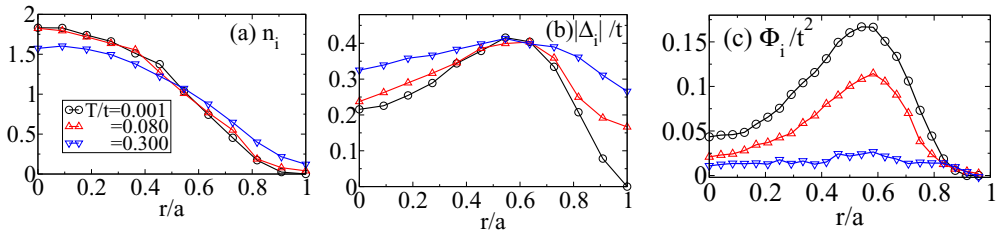

FIG. 2. (Color online) Spatial variation and temperature dependence at $U = 6t$, $V_c = 3t$. (a) density, $\langle\langle n_i \rangle\rangle$, (b) pairing field magnitude, $\langle|\Delta_i/t|\rangle$, (c) nearest neighbor pairing field correlation. All patterns are thermally averaged. r/a is the dimensionless normalized radial distance from the center along the diagonal.

increasing V_c due to appearance of low-frequency spectral weight and (2) the "coherence peak" and sharp gap edge are blurred. The decrease in the gap arises from the smaller pairing amplitude in regions which have density $n_i \to 0$ or $n_i \to 2$. We have explicitly checked this from the local density of states (LDOS). In fact at $n \sim 1.9$ the pairing gap in the flat system is $0.8t$, not very different from the threshold that we observe. The $n_i \sim 1$ region contributes to spectral weight at $|\omega| \gtrsim 2.5t$, consistent with results from the flat system. In a flat system the threshold, $\omega_{\rm gap}$, and the coherence peak location, $\omega_{\rm coh}$, coincide.

At $T \sim 0.08t$, Fig. 3(b), the DOS for $V_c = 0.1t$ and $V_c = t$ look very similar, with a reduction of $\omega_{\rm gap}$ from the $T = 0$ value and suppression of the coherence peak. The $V_c = 3t$ case also shows reduction of $\omega_{\rm gap}$ with respect to $T = 0$, but continues to be distinct compared to the weaker V_c cases. Since $\langle|\Delta_i|\rangle$ has not changed significantly with respect to $T = 0$ [Fig. 2(b)] these changes are attributable to phase disorder.

By the time $T = 0.3t$, Fig. 3(c), the DOS in the three cases are essentially similar, since the $\langle|\Delta_i|\rangle$ homogenizes even in the trap (Fig. 2). The density does continue to be inhomogeneous, affecting ϕ_i, but $|\Delta_i|$ is more important for the low-frequency spectrum.

IV. MOMENTUM-RESOLVED SPECTRAL FUNCTION

The momentum resolved spectral function, Fig. 4, is more dramatically affected by trapping. The 3×3 panel shows the spectrum $A(\mathbf{k},\omega)$. The formal definition in terms of HFBdG eigenstates is given in the Appendix. In each panel, the x axis corresponds to the $\mathbf{k}$ scan from $\{0,0\}$ to $\{\pi,\pi\}$, the y axis is the frequency ω, and $A(\mathbf{k},\omega)$ is color coded as indicated. The columns are for $V_c = 0.1t, t, 3t$ (left to right), the rows are $T = 0, 0.08t, 0.3t$ (top to bottom). The *size dependence* of our results is shown later.

The left column at $V_c = 0.1t$ shows the thermal evolution in an essentially flat system. (1) The top panel shows the ground state. Here $A(\mathbf{k},\omega) \approx u_{\mathbf{k}}^2 \delta(\omega - E_{\mathbf{k}}) + v_{\mathbf{k}}^2 \delta(\omega + E_{\mathbf{k}})$, where $E_{\mathbf{k}} = \sqrt{(\epsilon_{\mathbf{k}} - \mu)^2 + \Delta^2}$, $u_{\mathbf{k}}$ and $v_{\mathbf{k}}$ are the usual BCS coherence factors, $\epsilon_{\mathbf{k}}$ is the tight binding dispersion, and Δ is the uniform pairing amplitude. The two dispersing bands correspond to $\pm E_{\mathbf{k}}$, and one observes the expected "backbending" in the lower curve near $\mathbf{k} \sim \{\pi/2,\pi/2\}$ [30], where, for us, $\epsilon_{\mathbf{k}} \approx \mu$. (2) The middle panel shows that at $T = 0.08t$ coherent particle-hole mixing is almost lost. For $\mathbf{k} \sim \{\{0,0\} \to \{\pi/2,\pi/2\}\}$ the spectrum is mainly "particle-like," while for $\mathbf{k} \sim \{\{\pi/2,\pi/2\} \to \{\pi,\pi\}\}$ it is "hole-like." There is significant mixing only near $\mathbf{k} \sim \{\pi/2,\pi/2\}$. There is a faint surviving trace of the mean field, $\pm E_{\mathbf{k}}$, dispersion, the $+E_{\mathbf{k}}$ branch for $\mathbf{k} \sim \{0,0\}$, and the $-E_{\mathbf{k}}$ branch for $\mathbf{k} \sim \{\pi,\pi\}$. Effectively there are three branches in $A(\mathbf{k},\omega)$ at each $\mathbf{k}$. (3) The bottom panel shows that at $T = 0.3t$ there is no trace of the mean field $E_{\mathbf{k}}$, and the spectrum is an incoherent combination of upper and lower band features at all $\mathbf{k}$.

For $V_c = t$, the middle column, the moderate confinement already shows signatures in $A(\mathbf{k},\omega)$. (1) In the top panel, the $T = 0$ spectral functions are broad since $\mathbf{k}$ states overlap with multiple trap eigenstates. Low $\mathbf{k}$ states have large (and broad) weight in the lower band while $\mathbf{k} \sim \{\pi,\pi\}$ involves broad weight in the upper band. The gap between the upper and lower bands is still smallest at $\mathbf{k} \sim \{\pi/2,\pi/2\}$, and the backbending feature has not vanished. (2) At $T = 0.08t$ and $T = 0.3t$ the results are similar to what we saw for the flat case, with some extra (trap induced) broadening noted above.

The third column shows results at $V_c = 3t$ where the trap center density is $n_i \approx 2$. The ARPES differs qualitatively from the flat case. (1) At the top, at $T = 0$ the $A(\mathbf{k},\omega)$ is very broad since a large number of trap eigenstates overlap with $|\mathbf{k}\rangle$. The interband separation now has a *maximum* for $\mathbf{k} \sim \{\pi/2,\pi/2\}$ and is minimum for $\mathbf{k} \to \{0,0\}$ or $\{\pi,\pi\}$. This

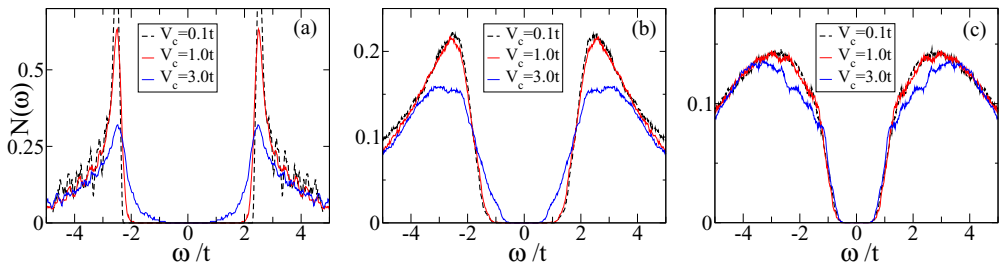

FIG. 3. (Color online) DOS for increasing degree of confinement at three temperatures: (a) $T = 0$, (b) $T = 0.08t$, and (c) $T = 0.3t$.

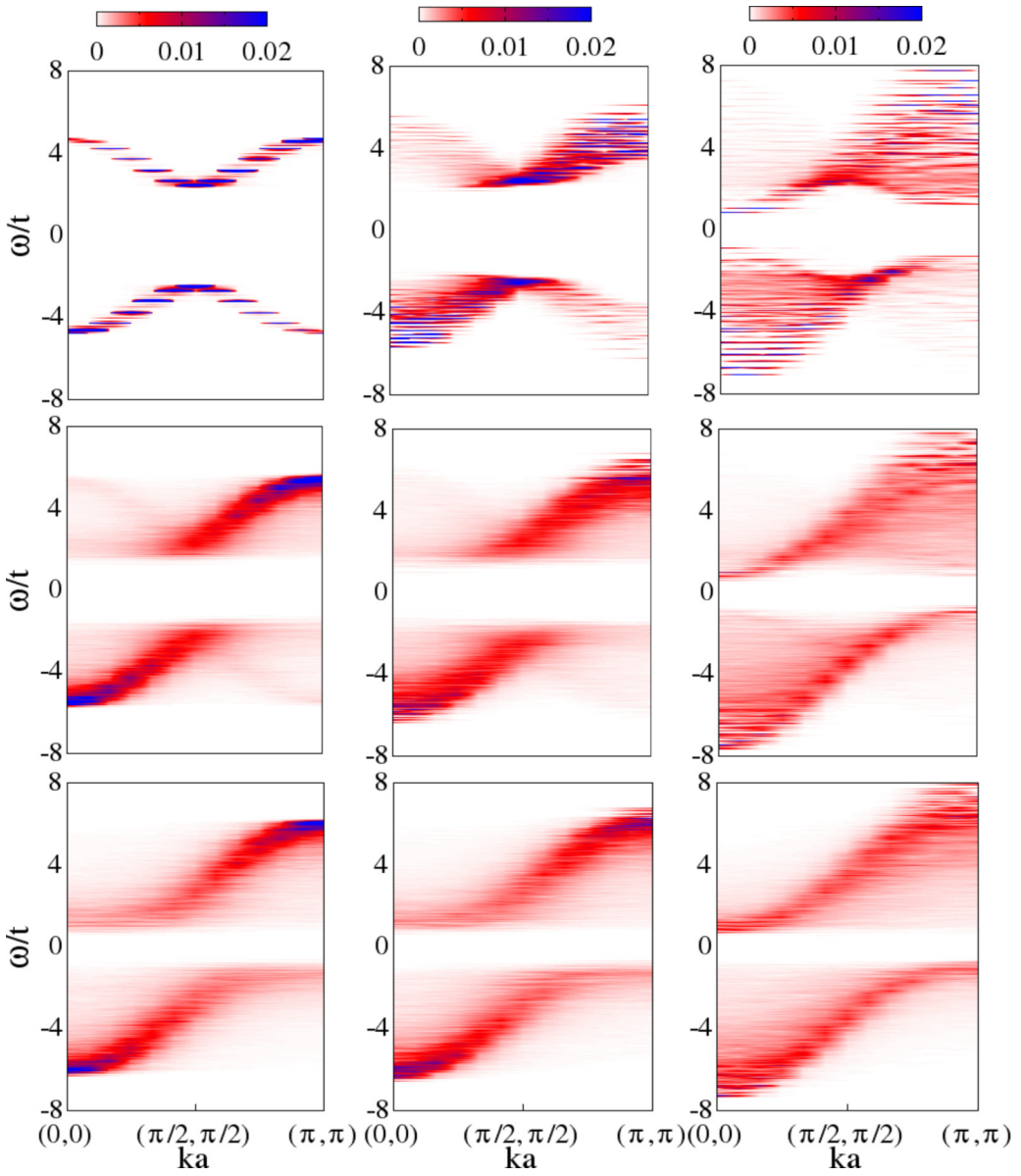

FIG. 4. (Color online) The spectral function $A(\mathbf{k},\omega)$ for a "diagonal scan" of momentum from $\mathbf{k}a = \{0,0\} \rightarrow \{\pi,\pi\}$. Along the row, V_c varies from $0.1t,t,3t$ (left to right). Down the column T varies from $0,0.08t,0.3t$. The T_c of the unconfined system is $\sim 0.14t$; at $V_c = 3t$ it is $\sim 0.1t$.

is a case of "forward bending" rather than backbending. If RF spectroscopy probes the edge of the lower band it would obtain a concave pattern, rather than the convex result that traditionally indicates a pairing gap. The gap, as is obvious from the full $A(\mathbf{k},\omega)$ is nevertheless present. (2) In the middle, at $T = 0.08t$ all gaps are smaller compared to $T = 0$ but the unusual $\mathbf{k}$ dependence persists. (3) In the bottom, at $0.3t$ there is only the hint of the $\mathbf{k}$ dependent gap observed at lower T. How do we relate these results to spatial structure?

The overall DOS is $N(\omega) = -(1/\pi) Im \sum_i G_{ii}(\omega)$, i.e., a sum of the local DOS over the system where $G_{ii}(\omega)$ is the local projection of the spin averaged fermion Green's function. If the density n_i were *slowly* varying, then as a starting approximation we could use $G_{ii}^{\rm trap}(\omega) \approx G^{\rm flat}(\omega, n = n_i)$. We have checked that this works reasonably even on our 24×24 system. The overall DOS is then given by $N(\omega) \approx \int dn\, P(n) N_{\rm flat}(\omega,n)$, where $N_{\rm flat}(\omega,n)$ is the flat system DOS at density n and the density distribution $P(n) = \frac{1}{N} \sum_i \delta(n - n_i)$ can be computed from the MC density profile.

This immediately creates a connection between the density (and auxiliary field) variation in the trap and the features observed in the DOS. The ARPES, however, involves the overlap $\langle \mathbf{k}|m\rangle$ of a plane wave state with a BdG eigenstate ψ_m. If all ψ_m were extended over the system, and overlap all $|\mathbf{k}\rangle$, the strange gap modulation with $\mathbf{k}$ would not arise.

We find that the BdG states are *radially localized to a remarkable degree*. Section V C shows typical real space and momentum space patterns for $V_c = 3.0t$. The lowest energy excitation at $T = 0$, at $E_m \sim 0.9t$, is localized near the corners, where $n_i \rightarrow 0$. This has Fourier modes only near $\mathbf{k} = \{0,0\}$. For $E_m \gtrsim 1.3t$ the excitations shift to the center of the trap and involve modes near $\mathbf{k} \sim \{\pi,\pi\}$. Only for $E_m \gtrsim 2.5t$, where the

BdG states have large weight on the $n_i \approx 1$ annulus do we see contribution at $\mathbf{k} \sim \{\pi/2,\pi/2\}$.

Although our system size is larger than accessible in typical DQMC studies, it is well below the $\sim 100 \times 100$ lattices used in experiments. This is where the local density approximation (LDA) to $P(n)$ becomes useful. LDA prescribes that $n_i^{\text{trap}} \approx n_{\text{flat}}(\mu_i)$, where $\mu_i = \mu - V_i$ and $n_{\text{flat}}(\mu)$ can be computed from DQMC or analytic approximations. In Sec. V D we compare the MC based ARPES data with results obtained using LDA on the same size. The agreement is remarkable. We extended this to a huge $\sim 200 \times 200$ system, and all the qualitative features of our original result survive.

V. DISCUSSION

A. Benchmarks

To benchmark our result we compare the superfluid transition temperature (T_c) obtained by our strategy to available DQMC results at density $n = 0.7$ on a 10×10 lattice for U/t varying from 2 to 8. Figure 5 compares our results to this benchmark. We capture the nonmonotonic character and the correct peak location, and our T_c estimate is within 10% of the DQMC result at all U/t. This is far superior to mean field theory, which would have generated a T_c growing monotonically with U/t, with an *order of magnitude overestimate* already at $U/t = 6$.

B. Origin of thermal behaviour

In Fig. 2 the mean value of $|\Delta_i|$ tends to become independent of position $\mathbf{r}_i$ with growing T, even though the density n_i remains inhomogeneous. This is related to the lower amplitude stiffness of regions with low $|\Delta|$ at $T = 0$ and has a direct correspondence with the behavior in flat systems. In Fig. 6 we have studied the mean value $\bar{\Delta}(n,T) = (1/N)\sum_i \langle|\Delta_i|\rangle_{n,T}$ in the flat system and discovered that although $\bar{\Delta}$ is strongly n dependent at $T = 0$, with a 70% variation as n changes from 1.0 to 0.1, at $T = 0.3t$ that variation is only $\sim$30%. This flat system effect shows up in the trap as a local amplitude stiffness that depends on the $T = 0$ magnitude of $|\Delta|$ in that region.

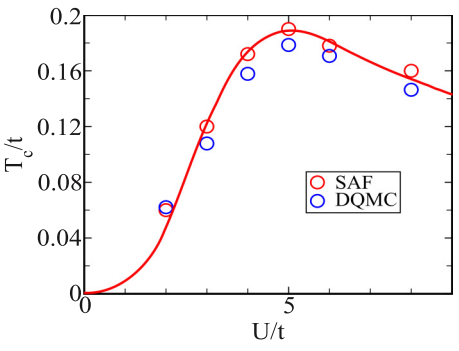

FIG. 5. (Color online) Comparison of superfluid T_c obtained within our static auxiliary field (SAF) scheme, with DQMC (Ref. [15]) for various values of interaction strength. The results are for a flat system with density $n = 0.7$ and lattice size 10×10.

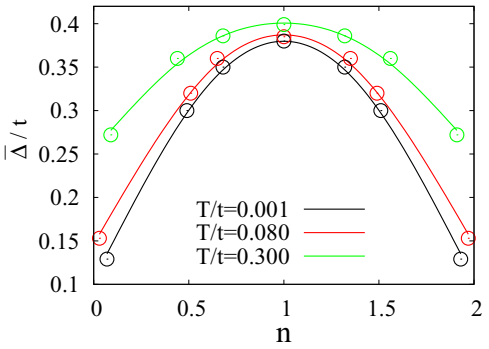

FIG. 6. (Color online) The thermal average of $|\Delta/t|$ on a "flat" system for varying density (n) and temperature (T). The $T = 0.001t$ result corresponds to mean field theory; the finite T results involve fluctuations within the SAF scheme.

C. Behaviour of Bogoliubov-de Gennes (BdG) wave functions

We analyzed the BdG wave functions in real space and in terms of their momentum content and show a few illustrative examples in Fig. 7 for $V_c = 3t$. BdG wave functions in real space have been represented by u_i, v_i and in momentum space as U_k, V_k. The center of the spatial maps is $\mathbf{r}_i = (0,0)$. For the momentum maps the center is $\mathbf{k} = (0,0)$, and the corners are $(\pm\pi,\pm\pi)$.

Our observations are the following: (1) The first row of Fig. 7 corresponds to the lowest energy excitation. One can see that (a) the state has large amplitude in the low-density region at the corners and (b) U_k and V_k are large near $\mathbf{k} = 0$. The low gap in $A(\mathbf{k} = 0,\omega)$ arises due to overlap with this excitation. (2) In the second row, $E = 1.326t$, higher up in the spectrum. This state (a) is mainly localized at the center of the trap, i.e., the highest density region, and (b) is the first state with significant $\mathbf{k} = (\pi,\pi)$ content. The $|\Delta_i|$ here is small, but larger than in the corner region. (3) Row 3 shows states with contribution at $\mathbf{k} = (\pi/2,\pi/2)$. These are spread over the system but have significant weight in the $n \approx 1$ annulus, where $|\Delta|$ at $T = 0$ is largest. The states are at significantly higher energy than the states in rows 1 and 2.

D. Extrapolation to large system size

Pushing the "local density" approach to the momentum resolved spectral function we checked the accuracy of this approach in capturing $A(\vec{k},\omega)$ in the trap. We computed the "local density" based spectral function $A^L_{\text{trap}}(\mathbf{k},\omega)$ as follows:

$$A^L_{\text{trap}}(\mathbf{k},\omega) = \int P(n) A_{\text{flat}}(n,\mathbf{k},\omega)\, dn. \tag{6}$$

This prescription is incomplete without specifying $P(n)$. The first approximation is to use the $P_{\text{MC}}(n)$ that emerges from the MC itself. This approach, although it does not require BdG solutions on the large system, still requires MC-generated data and is impractical on large sizes, $\sim 100 \times 100$, that are likely to be used in experiments. For that $P(n)$ itself needs to be approximated.

We tested the standard prescription that, for a slowly varying density field, one can relate n_i to a *local chemical*

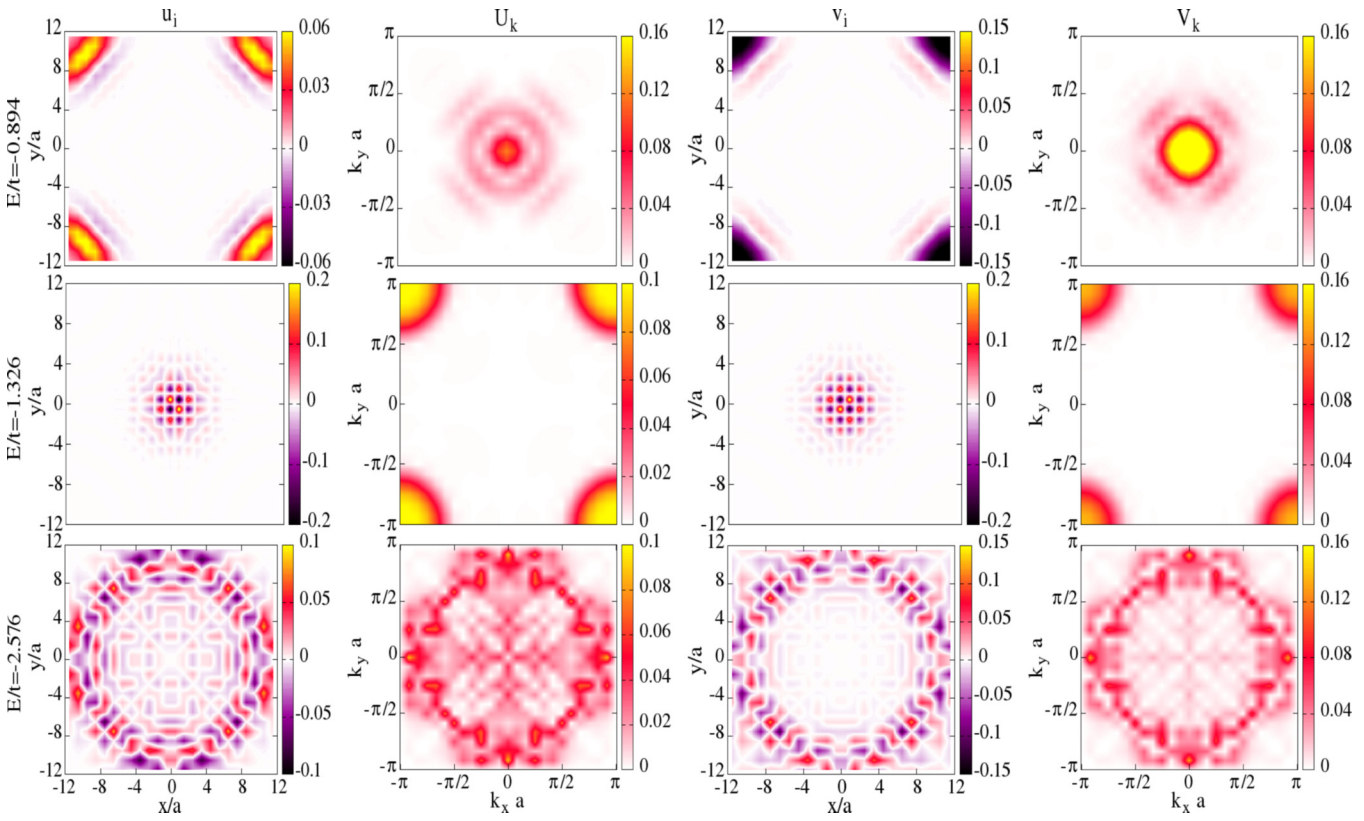

FIG. 7. (Color online) BdG eigenfunctions for three different excitation energies, along the row $u_i^m, U_{\mathbf{k}}^m, v_i^m, V_{\mathbf{k}}^m$. Along the column different m, starting with the lowest E_m.

potential $\mu_i = \mu - V_i$, where n_i and μ_i are related by the same equation of state as in the homogeneous system. That relation we infer from numerical results on the flat system. The $\mu_{\rm LDA}$ itself is fixed by requiring $\frac{1}{N}\sum_i n_i(\mu_i) = n_{\rm av}$. From n_i one can generate the "local density approximation" result $P_{\rm LDA}(n)$. This can be computed easily on any size, and we generated it on 24×24 and 192×192 lattices.

Figure 8 compares the full HFBdG spectral function at $V_c = 3t$ with three approximations (along the row) at $T = 0$. The first panel shows the HFBdG result for $A(\mathbf{k},\omega)$, while the second panel shows $A^L_{\rm trap}(\mathbf{k},\omega)$ based on $P_{\rm MC}(n)$ integration. The third panel shows $A^L_{\rm trap}(\mathbf{k},\omega)$ based on $P_{\rm LDA}(n)$ on a 24×24 lattice; the fourth panel shows the result on a 192×192 lattice. For the larger lattice the corner potential is kept at $V_c = 3t$, as in the small system, so that the larger and smaller systems are roughly equivalent. All the main features of the HFBdG based calculation survive in the $P(n)$-based result. We have checked that the correspondence works at finite temperature as well.

VI. CONCLUSIONS

We provide a solution to the angle-resolved spectral properties of attractive fermions on a lattice in the presence of confinement, crucial for any cold atom experiment. Even a moderate trapping potential creates a "core" with low pairing amplitude and generates spectral features that are widely

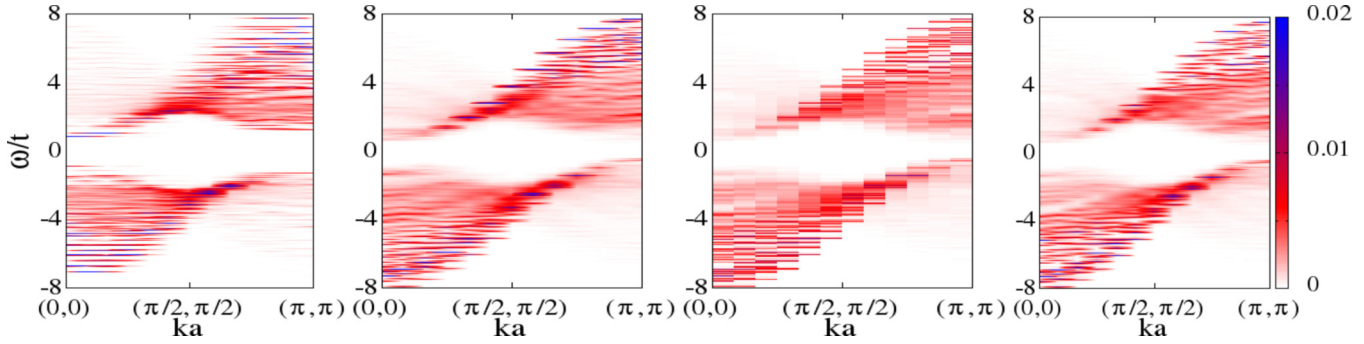

FIG. 8. (Color online) Comparison of the actual $A(\mathbf{k},\omega)$ (first column) with that based on $P(n)$ obtained from the full calculation (second column) and on $P(n)$ obtained from LDA scheme for 24×24 lattice (third column) and 192×192 lattice (fourth column). All the figures are for the ground state.

different from the well-studied "continuum" model and the "flat" Hubbard lattice. We point out a "forward bending" feature that would be the RF spectroscopy signature of a pairing gap, clarify the spatial origin of this feature, and illustrate a scheme that allows access to the spectrum on very large experimentally realized lattices. By analyzing the spatial character of the BdG states and their momentum content we have shown that the low-density region of the trap induces a smaller gap at low momentum while the high-density part of the trap contributes a smaller gap at high momentum.

ACKNOWLEDGMENTS

We acknowledge use of the HPC Cluster at HRI. P.M. acknowledges support from a DAE-SRC Outstanding Research Investigator Award.

APPENDIX: FORMAL DEFINITION OF $A(\mathbf{k},\omega)$

The spectral function $A(\mathbf{k},\omega)$ for a given configuration of Δ_i,ϕ_i has been calculated via the following expression:

$$A(\mathbf{k},\omega) = \sum_{n,E_n\geqslant 0} [|u_n(\mathbf{k})|^2\delta(\omega - E_n) + |v_n(\mathbf{k})|^2\delta(\omega + E_n)], \tag{A1}$$

where

$$u_n(\mathbf{k}) = \frac{1}{N^{1/2}}\sum_{i=1}^{N} e^{i\mathbf{k}\cdot\vec{r}_i}u_n(\vec{r}_i),$$

$$v_n(\mathbf{k}) = \frac{1}{N^{1/2}}\sum_{i=1}^{N} e^{i\mathbf{k}\cdot\vec{r}_i}v_n(\vec{r}_i).$$

To get the final $A(\mathbf{k},\omega)$ it has been averaged over many equilibrium configuration of Δ_i,ϕ_i.

[1] D. Jaksch, C. Bruder, J. I. Cirac, C. W. Gardiner, and P. Zoller, Phys. Rev. Lett. **81**, 3108 (1998).
[2] T. Esslinger, Annu. Rev. Condens. Matter Phys. **1**, 129 (2010).
[3] I. Bloch, Nat. Phys. **1**, 23 (2005).
[4] D. Jaksch and P. Zoller, Ann. Phys. (NY) **315**, 52 (2005).
[5] M. Köhl, H. Moritz, T. Stöferle, K. Günter, and T. Esslinger, Phys. Rev. Lett. **94**, 080403 (2005).
[6] U. Schneider *et al.*, Science **322**, 1520 (2008).
[7] R. Jordens *et al.*, Nature (London) **455**, 204 (2008).
[8] J. K. Chin *et al.*, Nature (London) **443**, 961 (2006).
[9] L. Hackermuller *et al.*, Science **327**, 1621 (2010).
[10] E. V. Gorelik, I. Titvinidze, W. Hofstetter, M. Snoek, and N. Blümer, Phys. Rev. Lett. **105**, 065301 (2010).
[11] S. Chiesa, C. N. Varney, M. Rigol, and R. T. Scalettar, Phys. Rev. Lett. **106**, 035301 (2011).
[12] W. Hofstetter *et al.*, Phys. Rev. Lett. **89**, 220407 (2002).
[13] D. Greif *et al.*, Science **340**, 1307 (2013).
[14] R. T. Scalettar, E. Y. Loh, J. E. Gubernatis, A. Moreo, S. R. White, D. J. Scalapino, R. L. Sugar, and E. Dagotto, Phys. Rev. Lett. **62**, 1407 (1989).
[15] A. Moreo and D. J. Scalapino, Phys. Rev. Lett. **66**, 946 (1991).
[16] T. Paiva, R. Scalettar, M. Randeria, and N. Trivedi, Phys. Rev. Lett. **104**, 066406 (2010).
[17] J. T. Stewart *et al.*, Nature (London) **454**, 744 (2008); Bernd Fröhlich *et al.*, Phys. Rev. Lett. **106**, 105301 (2011).
[18] J. P. Gaebler *et al.*, Nat. Phys. **6**, 569 (2010); M. Feld *et al.*, Nature (London) **480**, 75 (2011).
[19] A. Koga, T. Higashiyama, K. Inaba, S. Suga, and N. Kawakami, Phys. Rev. A **79**, 013607 (2009).
[20] E. Assmann, S. Chiesa, G. G. Batrouni, H. G. Evertz, and R. T. Scalettar, Phys. Rev. B **85**, 014509 (2012). This involves possibly the largest size explored within DQMC, 30×30, but focuses on thermodynamics and equal time correlations.
[21] D. Rost, E. V. Gorelik, F. Assaad, and N. Blümer, Phys. Rev. B **86**, 155109 (2012), does a systematic size dependence of the spectral functions of the *repulsive* Hubbard model at half-filling, in the absence of any trap.
[22] Y. Dubi, Y. Meir, and Y. Avishai, Nature **449**, 876 (2007).
[23] M. Mayr, G. Alvarez, C. Şen, and E. Dagotto, Phys. Rev. Lett. **94**, 217001 (2005).
[24] S. Kumar and P. Majumdar, Eur. Phys. J. B **50**, 571 (2006).
[25] S. De Palo, C. Castellani, C. DiCastro, and B. K. Chakraverty, Phys. Rev. B **60**, 564 (1999).
[26] For multichannel decomposition the sum of squares of couplings in the two channels should equal unity.
[27] A. Ghosal, M. Randeria, and N. Trivedi, Phys. Rev. B **65**, 014501 (2001).
[28] P. G. de Gennes, *Superconductivity of Metals and Alloys* (Addison Wesley, New York, 1989).
[29] S. Datta and P. Majumdar (unpublished).
[30] J. M. Singer, T. Schneider, and P. F. Meier, Eur. Phys. J. B **7**, 37 (1999).